Electronic Supplementary Material (ESI) for Materials Advances.

Supporting Information for

A heterogeneous reaction strategy towards the general synthesis of 2D non-layered nanomaterials

Wenjing Qin, Hao Liu, Jiahui Liu, Jiangbo Yuan, Cong Wei, and Qun Xu**

College of Materials Science and Engineering, Zhengzhou University, Zhengzhou 450001, China

E-mail: weicong@zzu.edu.cn; qunxu@zzu.edu.cn

Materials and experimental details

1. Materials.

Thiourea, titanous sulfate, aluminum sulfate, absolute ethyl alcohol, ammonium hydroxide and n-hexane were purchased from Shanghai Hushi Laboratorial Equipment Co.,Ltd. Cadmium chloride and bismuth oxide were purchased from Shanghai Aladdin Biochemical Technology Co.,Ltd. Copper sulfate were purchased from Accela ChemBio Co., Ltd. Sodium carbonate were purchased from J&K Scientific Ltd. PEG200 were purchased from Tianjin Kermel Chemical Reagent Co.,Ltd.

2. Synthesis of the two-dimensional non-layered materials.

Synthesis procedure of 2D Bi_2S_3 nanosheets.

2D Bi_2S_3 nanosheets was synthesized via a solid-solid heterogeneous reaction. In a routine process, 1 g thiourea crystals and 0.2 g bismuth oxide were added into a mortar and mixed for 30 minutes. And then, the mixture was added into an autoclave and heat it for 1 hour at 180 ℃. After finishing the reaction, the mixture were washed sequentially with sulphuric acid and distilled water for three times. Finally, 2D-Bi_2S_3 nanosheets were collected by centrifugation and dried at 60 ℃ in a vacuum drying oven.

Synthesis procedure of 2D CuO nanosheets.

2D CuO nanosheets was synthesized via a solid-liquid-solid heterogeneous reaction. In a routine process, 1 g copper sulfate and 0.2 g sodium carbonate were added into a mortar and mixed for 30 minutes. And then, transfer the mixture into an autoclave and add 100 μL n-hexane to accelerate the diffusion of the precursors, which is key point for this reaction. The reactor was sealed and heated for 8 h at 160 ℃. After finishing the reaction, the mixture were washed sequentially with deionized water, ammonium hydroxide and deionized water for three times. Finally, 2D-CuO nanosheets were collected by centrifugation and dried at 60 ℃ in a vacuum drying oven.

Synthesis procedure of 2D TiO_2 nanosheets.

2D TiO_2 nanosheets was synthesized via a solid-solid heterogeneous reaction. In a routine process, 0.2 g titanous sulfate and 1 g sodium carbonate were added into a mortar and mixed for 30 minutes. And then, add the mixture into a porcelain boat and heat it for 0.5 h at 500 ℃. After finishing the reaction, the mixture were washed sequentially with sulphuric acid and distilled water for three times. Finally, 2D-TiO_2 nanosheets were collected by centrifugation and dried at 60 ℃ in a vacuum drying oven.

Synthesis procedure of 2D Al_2O_3 nanosheets.

2D Al_2O_3 nanosheets was synthesized via a solid-solid heterogeneous reaction. In a routine process, 0.2 g aluminum sulfate and 1 g sodium carbonate were added into a mortar and mixed for 30 minutes. And then, add the mixture into a porcelain boat and heat it for 4 h at 600 ℃. After finishing the reaction, the

mixture were washed sequentially with distilled water for three times. Finally, 2D-Al_2O_3 nanosheets were collected by centrifugation and dried at 60 ℃ in a vacuum drying oven.

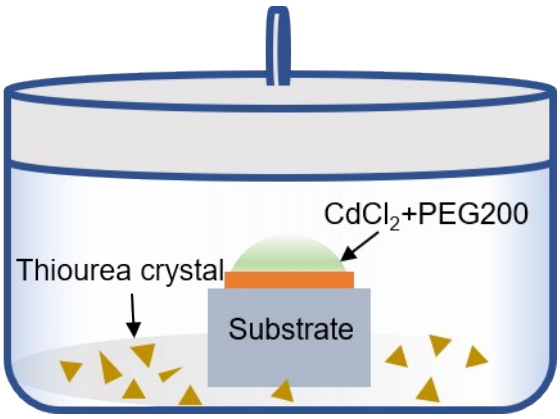

Figure S1. Scheme of the gas-liquid reaction set-up for the growth of CdS nanosheets.

As shown in Figure S1, $CdCl_2$/PEG200 solution was injected onto a substrate, which was put into a sealed beaker with thiourea at the bottom. Under thermal treatment, gaseous thiourea molecules would diffuse and encounter with the liquid Cd precursor at the interface, forming a typical gas-liquid reaction.

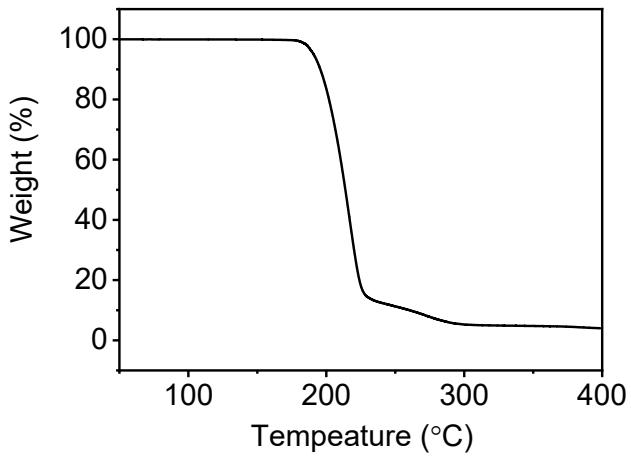

Figure S2. TG curve of the thiourea molecules.

As the temperature raised to 175-300 °C, thiourea crystal lost its weight quickly and the ultimate weightlessness turned out to be 95%, indicating that thiourea molecules would undergo significant gasification and pyrolysis when the temperature exceeds 175 °C.[1]

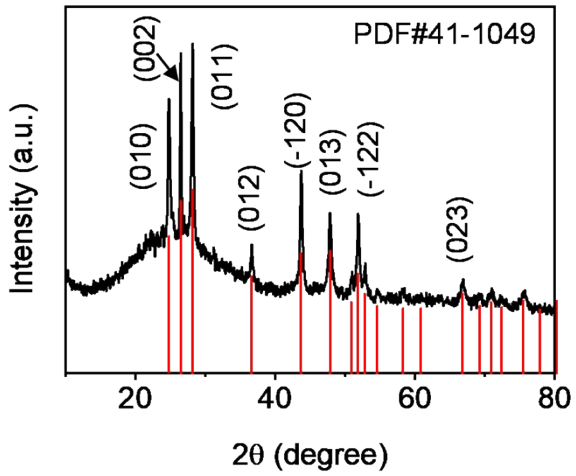

Figure S3. XRD patterns of the bulk CdS crystal.

All of the diffraction peaks can be indexed to the hexagonal phase of cadmium sulfide with lattice parameters of a = 4.14 Å, b = 4.14 Å and c =6.71 Å. This result clearly shows that the samples possessed only the hexagonal CdS phase, which matches well with the standard data file (PDF#41-1049). As labeled in the figure, the main peaks are assigned to be (010), (002), (011), (012), (-120), (013), (-122) and (023) lattice planes of CdS, respectively. In comparison, the diffraction peak of (-120) plane disappears in the XRD patterns of the 2D samples (Figure 1g), further confirming the exposed face of the as-prepared 2D nanosheets correspond to the (-120) plane of CdS crystal.

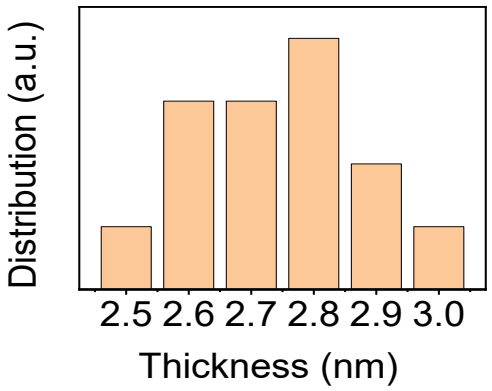

Figure S4. The thickness distribution histograms of the typical CdS nanosheets.

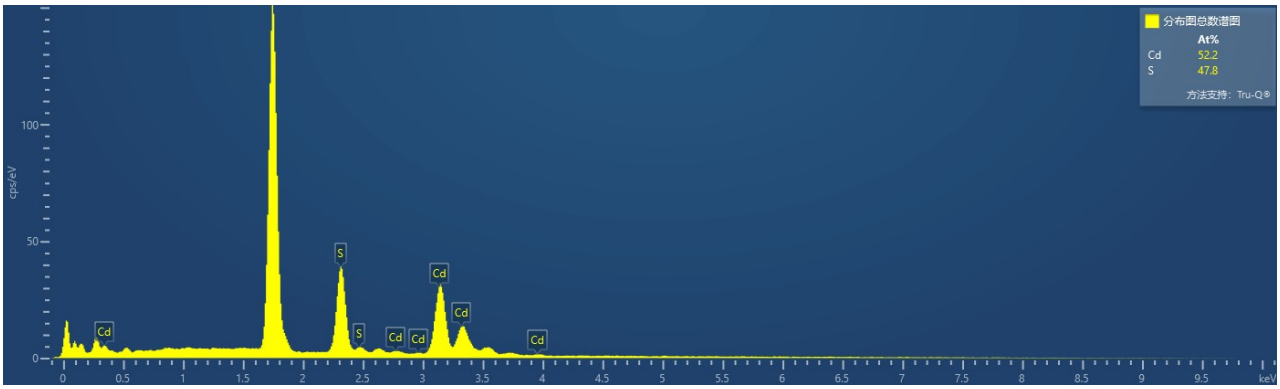

Figure S5. Energy-dispersive X-ray spectrum of the obtained CdS nanosheets.

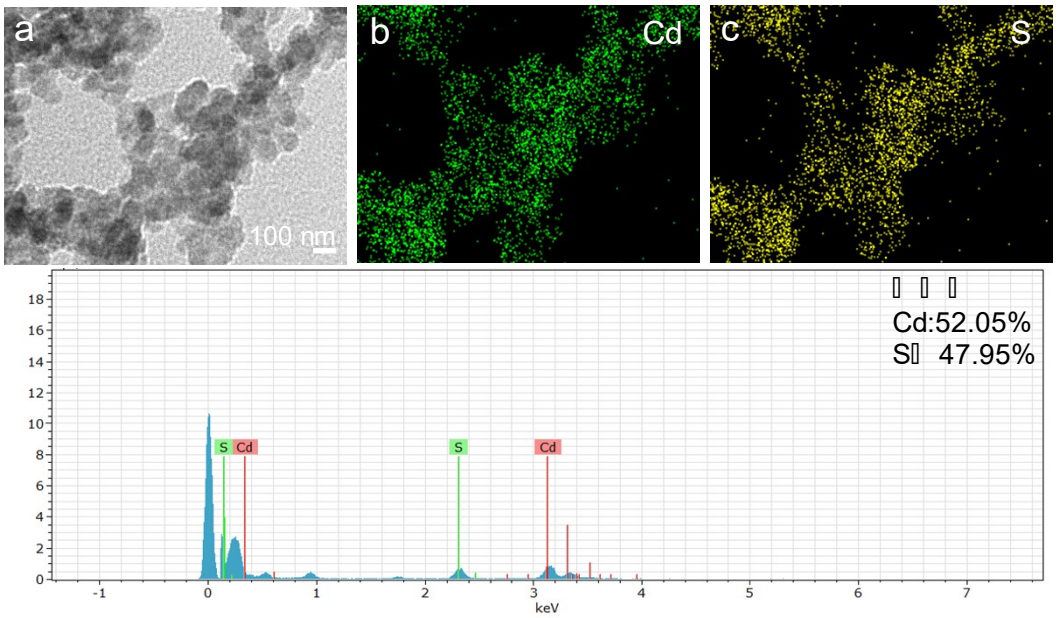

Figure S6. (a-c) TEM image and EDS elemental mapping of Cd and S for the obtained single CdS nanosheet. (d) Energy-dispersive X-ray spectrum of the single CdS nanosheet.

The elemental mapping images of the non-stacked cadmium sulfide nanosheets demonstrated the uniform distribution of Cd and S elements. And the EDS spectrum in Figure S6 showed an atomic ratio closing to 1:1, in agreement with the stoichiometric ratio of CdS crystal.

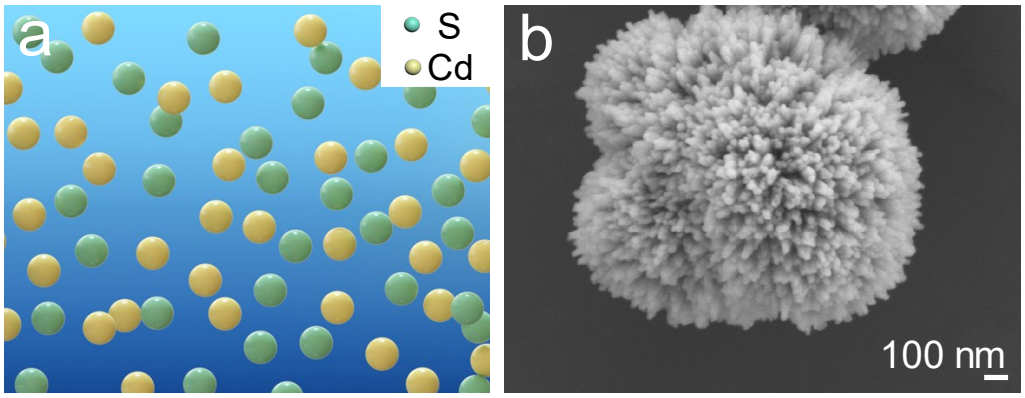

Figure S7. (a) Schematic illustration of the homogeneous synthesis of CdS. (b) SEM image of CdS crystals obtained via a homogeneous reaction.

A homogeneous reaction system was carried out as a control experiment, Cd and S precursors are well mixed in water and can migrate freely (Figure S7a). The morphology of the product is mainly determined by the surface lattice energy.[2, 3] As shown in Figure S7b, only rod-like rather than 2D shaped crystals were obtained, conforming the heterogeneous reaction system was the key point for the formation of the 2D CdS nanosheets.

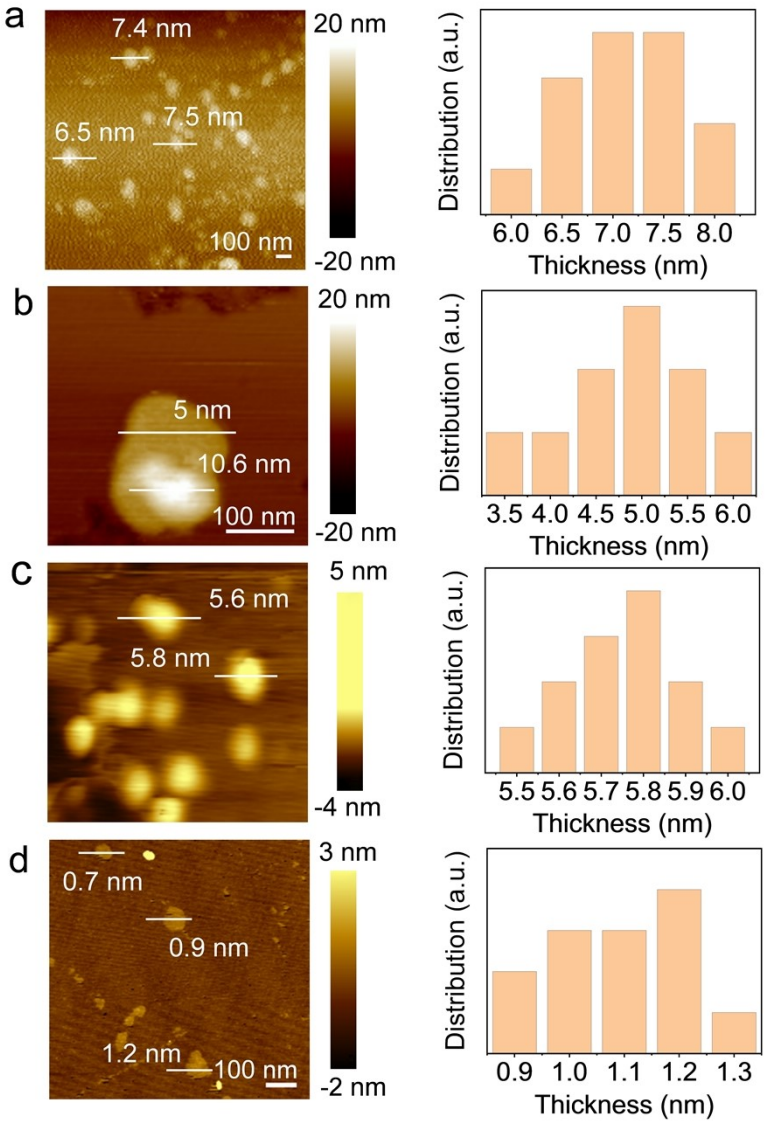

Figure S8. AFM images and thickness distribution histograms of the heterogeneous synthesized 2D nanosheets (a) Bi_2S_3, (b) CuO, (c) TiO_2 and (d) Al_2O_3.

A representative image of the synthesized 2D Bi_2S_3 nanosheets is shown in Figure S8a, which reveals a mainly thickness of 6.5 to 8 nm with lateral size up to 100 nm. Likewise, the AFM image in Figure S8b indicates that the thicknesses of the CuO nanosheets are approximately 4.5 to 5.5 nm. The thickness of TiO_2 nanosheets in Figure S8c vary from 5.6 to 5.9 nm. And the thicknesses for the relatively thin Al_2O_3 samples are approximately 0.7 to 1.2 nm with a lateral size up to 100 nm. All of them have the typical 2D morphology.

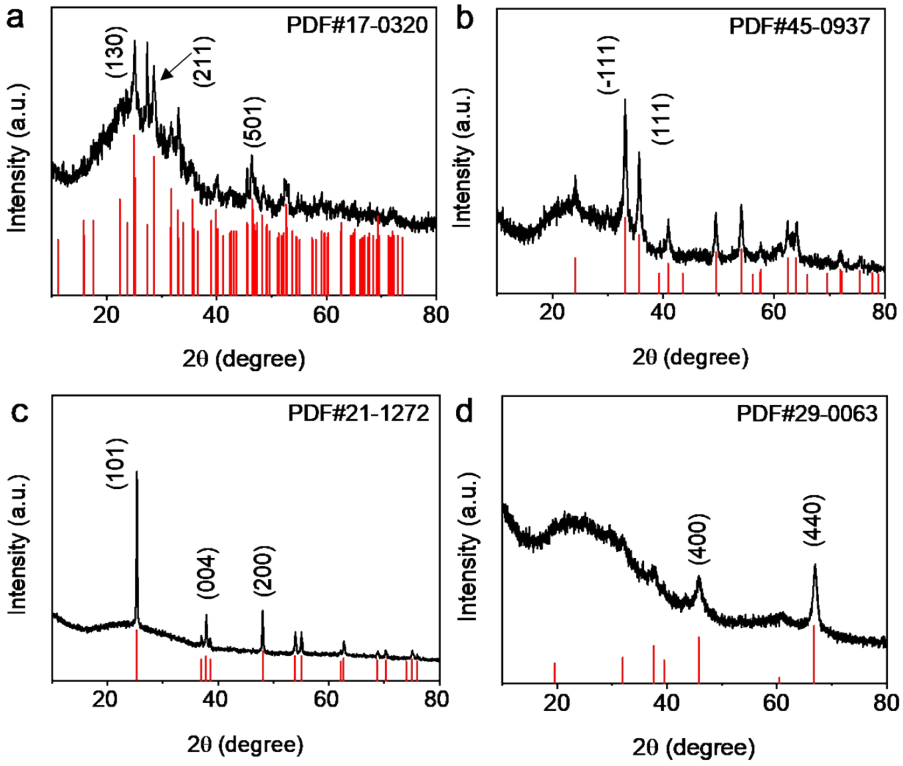

Figure S9. XRD patterns of the as-synthesized 2D nanosheets. (a) orthorhombic Bi_2S_3, (b) monoclinic CuO, (c) tetragonal TiO_2 and (d) cubic Al_2O_3.

As shown in Figure S9a, the patterns of the Bi_2S_3 nanoplates can be indexed to bismuthinite phase with lattice parameters of a = 11.14 Å, b = 11.30 Å, c = 3.98 Å (PDF# 17-0320). The primary diffraction peaks can be indexed to the (130), (211) and (501) planes of orthorhombic Bi_2S_3, respectively. Similarly, the patterns of the CuO nanoplates (Figure S9b) can be indexed to tenorite phase with lattice parameters of a = 4.68Å, b = 3.42 Å and c = 5.13 Å (PDF# 45-0937). The primary diffraction peaks can be indexed to the (-111) and (111) planes of monoclinic CuO, respectively.The patterns of the TiO_2 nanoplates in Figure S7c can be indexed to anatase phase with lattice parameters of a = 3.78 Å, b = 3.78 Å and c = 9.51 Å (PDF# 21-1272). The primary diffraction peaks can be indexed to the (101), (004) and (200) planes of tetragonal TiO_2, respectively. And the patterns of Al_2O_3 nanoplates in Figure S7d can be indexed to aluminum oxide phase with lattice parameters of a = 7.92 Å, b = 7.92 Å and c = 7.92 Å (PDF# 29-0063). The primary diffraction peaks can be indexed to (400) and (440) planes of cubic Al_2O_3, respectively. All of synthesized nanosheets demonstrate clear diffraction peaks, indicating that their intrinsic non-layered lattices are well preserved.

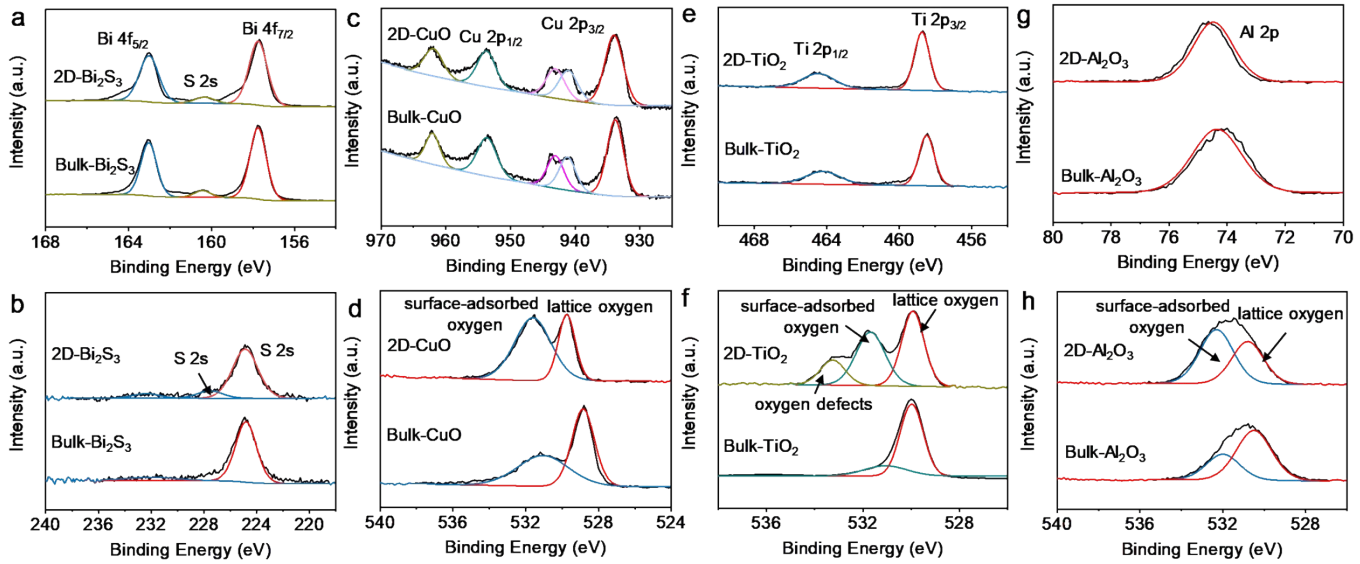

Figure S10. Surface chemical states of the ultrathin 2D nanosheets and their bulk phases. Bi 4f (a) and S 2s (b) spectra of 2D and bulk Bi_2S_3. Cu 2p (c) and O1s (d) spectra of 2D and bulk CuO. Ti 2p (e) and O 1s (f) spectra of 2D and bulk TiO_2. Al 2p (g) and O 1s (h) spectra of 2D and bulk Al_2O_3.

In high-resolution XPS spectra, Bi 4f, Cu 2p, Ti 2p and Al 2p signals can be clearly observed for both as-prepared nanosheets and bulk counterparts (as shown in Figure S10a, c, e, g), indicating the unchanged valence states of metal element in the 2D samples. However, a new fitting peak of S 2s appears at higher binding energy of 277.7 eV in the spectra of 2D Bi_2S_3 nanosheets (Figure S10b). And the content of absorbed oxygen in 2D CuO, TiO_2 and Al_2O_3 nanosheets also exhibits significant increase compared with their bulk counterparts (Figure S10d, f, h). These are resulted from the strong chemisorption capability of the abundant dangling bonds on their surface,[4, 5] which is a typical feature of atomically thin non-layered nanomaterials, further confirming their 2D feature.

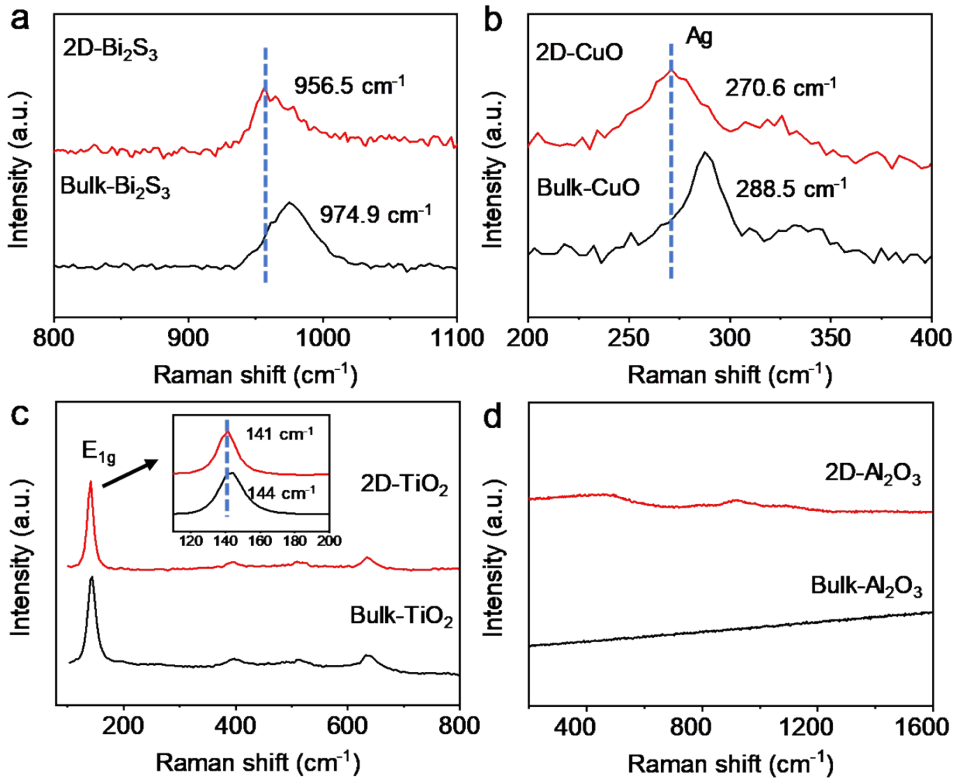

Figure S11. Raman spectra of the as-prepared 2D nanosheets and their bulk phases. (a) Bi_2S_3, (b) CuO, (c) TiO_2 and (d) Al_2O_3.

Compared with the bulk counterparts, the Raman scattering peak of 2D Bi_2S_3 nanosheets exhibits a 18 eV red shift (Figure S11a), and 18 eV for CuO (Figure S11b), 3 eV for TiO_2 (Figure S11c). Gamma-Al_2O_3 do not exhibit any peaks in the Raman spectra (Figure S11d). The distinct red shifts are resulted from the attenuation of the bond oscillator strength induced by the abundant surface dangling bonds, further confirming the 2D non-layered structure of the as-prepared samples.

References：

1. Z. D. Wang, M. Yoshida and B. George, *Theor. Chem.*, 2013, **1017**, 91-98.
2. W. Niu and G. Xu, *Nano Today*, 2011, **6**, 265-285.
3. N. Tian, Z.-Y. Zhou, S.-G. Sun, Y. Ding and Z. L. Wang, *Science*, 2007, **316**, 732-735.
4. H. Wu, X. Lu, G. Zheng and G. W. Ho, *Adv. Energy Mater.*, 2018, **8**, 1702704.
5. I. H. Kwak, H. S. Im, D. M. Jang, Y. W. Kim, K. Park, Y. R. Lim, E. H. Cha and J. Park, *ACS Appl. Mater. Interfaces*, 2016, **8**, 5327-5334.